ROYAL SOCIETY
OF CHEMISTRY

PAPER

Check for updates

Homoleptic complexes of vanadium and N-heterocycles made *via* oxidation of vanadium nanoparticles

Lena Baumgärtner and Claus Feldmann ⓘD *

The four homoleptic coordination compounds [NaV(cbz)$_4$] (**1**), [V(bipy)$_3$] (**2**), [V(phen)$_3$] (**3**), and [V (Hai)$_3$(ai)$_2$]·0.5 tol (**4**) are prepared by the reaction of vanadium metal (V(0)) nanoparticles (mean size: 1.6 ± 0.3 nm) with the sterically demanding N–H-acidic/non-N–H-acidic, chelating/non-chelating aromatic N-heterocycles carbazole (Hcbz), 2,2′-bipyridine (bipy), 1,10-phenanthroline (phen), and 7-azaindole (Hai). The V(0) nanoparticles are used as a reactive starting material to perform redox reactions with the N-heterocycles in toluene (tol) at 80–120 °C. The V(0) nanoparticles and the compounds **1–4** are characterized by X-ray diffraction (single crystals and powders), electron microscopy (TEM and STEM), spectroscopic methods (FT-IR and UV-Vis), and thermal analysis (TG). Besides the first use of V(0) nanoparticles in reactions with N-heterocycles, the underlying redox reactions result in new homoleptic V(II)/V(III) coordination compounds with the respective N-heterocycles as sole ligands. All coordinated N-heterocycles serve as monovalent anions with the N–H-acidic Hcbz and Hai being deprotonated leading to the formation of hydrogen, whereas the non-N–H-acidic bipy and phen are directly reduced with the oxidation of vanadium. Most interesting is compound **4** with three different coordination scenarios of the Hai/ai$^-$ ligand, resulting in a composition [V(η^1-Hai)$_3$(η^2-ai)(η^1-ai)]·0.5tol, which is observed here for the first time.

1. Introduction

Base-metal nanoparticles as well as their reactivity and reactions have generally attracted our interest in recent years.[1] To this end, we developed several liquid-phase syntheses strategies, including microemulsions in liquid ammonia,[1a] sodium-driven reduction in liquid ammonia,[1b] and lithium/sodium pyridinyl-driven reduction in pyridine.[1c] In particular, the reduction of metal halides by alkali-metal naphthalides ([LiNaph], [NaNaph]) in THF has been proven to be a highly versatile route to obtain group 3–6 transition metals and all lanthanide metals (La to Lu) as nanoparticles with sizes of 1–5 nm.[2] Besides the synthesis of these base-metal nanoparticles, many for the first time, we examined their reactivity and reactions, starting with small-molecule oxidants (O$_2$, S$_8$, NH$_3$, ROH, *etc.*),[2] followed by sterically demanding O–H/N–H-acidic alcohols and amines, cyclic ethers[3] and species featuring metal–metal interactions and cluster compounds.[4] Moreover, material properties such as hydrogen sorption, photocatalytic water splitting, or catalytic hydrogenation were studied.[5]

To evaluate the reactivity and reactions of base-metal nanoparticles, V(0) nanoparticles proved particularly advantageous as both their reactivity and the oxophilic character of vanadium are moderate.[4b,6] However, knowledge of V(0) nanoparticles remained limited for a long time. Thus, V(0) particles were only prepared by gas-phase methods, resulting in large sizes (>50 nm) with significant aggregation and oxygen contamination.[7] To stabilize metallic vanadium against oxidation, core@shell structures with a vanadium carbide shell for passivation were reported.[8] The well-known option to prepare metal nanoparticles *via* thermal decomposition of metal carbonyls is not applicable here as vanadium carbonyls are much less stable than other transition-metal carbonyls.[9] Therefore, a reliable synthesis – especially in the liquid phase – of small-sized V(0) nanoparticles (<10 nm) was unknown.

In the following, we use V(0) nanoparticles (1.6 ± 0.3 nm in diameter) that were prepared by the reduction of VCl$_3$ with [LiNaph]/[NaNaph] in THF to evaluate their reactivity and reactions with the aromatic N-heterocycles carbazole (Hcbz), 2,2′-bipyridine (bipy), 1,10-phenanthroline (phen), and 7-azaindole (Hai). Besides the realization of new compounds, we aim to examine the underlying redox process and resulting coordinative scenarios of different N–H-acidic/non-N–H-acidic, chelating/non-chelating aromatic N-heterocycles. This redox approach resulted in four homoleptic coordination com-

Institute of Inorganic Chemistry, Karlsruhe Institute of Technology (KIT), Engesserstrasse 15, D-76131 Karlsruhe, Germany. E-mail: claus.feldmann@kit.edu

pounds of vanadium with the respective N-heterocycles as sole ligands.

2. Experimental section

2.1 General

All reactions and sample handling were carried out under a dried argon atmosphere using standard Schlenk techniques or glove boxes. Reactions were performed in Schlenk flasks and glass ampoules that were evacuated ($p < 10^{-3}$ mbar), heated, and flashed with argon three times prior to use. The starting materials, VCl_3 (97%, Sigma-Aldrich), lithium metal (99%, Sigma-Aldrich), sodium metal (99%, Sigma-Aldrich), naphthalene (naph, 99%, Sigma-Aldrich), 2,2′-bipyridine (bipy, 99%, Sigma-Aldrich), 1,10-phenanthroline (phen, 99%, Sigma-Aldrich), carbazole (Hcbz, 95%, Sigma-Aldrich) and 7-azaindole (Hai, 98%, Sigma-Aldrich) were used as received. Tetrahydrofuran (THF, 99%, Seulberger) was distilled over potassium. Toluene (tol, 99%, Seulberger) was distilled over sodium. All compounds were handled and stored in argon-filled glove boxes (MBraun Unilab, $c(O_2, H_2O) < 0.1$ ppm).

2.2 Synthesis of compounds

V(0) nanoparticles. The synthesis of V(0) nanoparticles was performed according to a previous report.[2] Accordingly, 125.8 mg of VCl_3 (0.80 mmol), 16.7 mg of lithium (2.40 mmol) or 55.5 mg sodium (2.40 mmol), and 323.0 mg of naphthalene (2.52 mmol) were stirred in 15 mL of THF for 12 hours at ambient temperature resulting in a deep black suspension. The as-prepared V(0) nanoparticles were separated by centrifugation (22 000 rpm) and purified by resuspending/centrifugating in/from 10 mL of THF to remove excess starting materials. Whereas LiCl is readily soluble in THF, NaCl has poor solubility. Because both LiCl and NaCl are usually not included in the product compounds,[2–6] we intended to reduce efforts and time of purification (i.e. multiple centrifugation cycles in a glovebox) and reduce the number of redispersion/centrifugation steps in/from THF to just one purification step. Finally, the V(0) nanoparticles were dried under reduced pressure and at room temperature to obtain powder samples with a yield of about 70%. Losses are mainly caused by incomplete centrifugation.

[NaV(cbz)₄] (1). 32.6 mg (0.635 mmol) of the as-prepared V(0) nanoparticles, 167.2 mg of carbazole (Hcbz, 1.50 mmol), and 0.5 mL of toluene were sealed in a glass ampoule and heated to 120 °C for three weeks. A certain excess of V(0) nanoparticles with regard to the stoichiometry of the redox reaction was applied to maintain reducing conditions and to account for V(0) nanoparticles that agglomerate and become less reactive over the time of the reaction. After cooling to room temperature, black crystals of **1** were obtained in about 30% yield (relative to the amount of Hcbz).

[V(bipy)₃] (2). 32.6 mg (0.635 mmol) of the as-prepared V(0) nanoparticles, 193.6 mg of 2,2′-bipyridine (bipy, 1.04 mmol) and 0.5 mL of toluene were sealed in a glass ampoule and

heated to 80 °C for 7 days. A certain excess of V(0) nanoparticles with regard to the stoichiometry of the redox reaction was applied to maintain reducing conditions and to account for V(0) nanoparticles that agglomerate and become less reactive over the time of the reaction. After cooling to room temperature, black crystals of **2** were obtained in about 60% yield (relative to the amount of bipy).

[V(phen)₃] (3). 32.6 mg (0.635 mmol) of the as-prepared V(0) nanoparticles, 273.1 mg of 1,10-phenanthroline (phen, 1.50 mmol) and 0.5 mL of toluene were sealed in a glass ampoule and heated to 100 °C for 7 days. A certain excess of V(0) nanoparticles with regard to the stoichiometry of the redox reaction was applied to maintain reducing conditions and to account for V(0) nanoparticles that agglomerate and become less reactive over the time of the reaction. After cooling to room temperature, black crystals of **3** were obtained in about 70% yield (relative to the amount of phen).

[V(η^1-Hai)₃(η^2-ai)(η^1-ai)]·tol (4). 32.6 mg (0.635 mmol) of the as-prepared V(0) nanoparticles, 92.5 mg of 7-azaindole (Hai, 0.79 mmol) and 0.5 mL of toluene were sealed in a glass ampoule and heated to 100 °C for three weeks. A certain excess of V(0) nanoparticles with regard to the stoichiometry of the redox reaction was applied to maintain reducing conditions and to account for V(0) nanoparticles that agglomerate and become less reactive over the time of the reaction. After cooling to room temperature, dark red crystals of **4** were obtained in about 70% yield (relative to the amount of Hai).

Handling the compounds. The title compounds **1–4** are sensitive to air and moisture and need to be handled under inert conditions (see the SI).

2.3 Analytical methods

Detailed information regarding the applied analytical methods can be found in the SI.

3. Results and discussion

3.1 Vanadium metal nanoparticles

The synthesis of V(0) nanoparticles was performed following our previously published synthesis strategy.[4b,6] Accordingly, VCl_3 was dissolved in THF and reduced by [LiNaph] or [NaNaph] at room temperature (Fig. 1a). Since the reduction is very fast whereas the dissolution of VCl_3 in THF is very slow, the synthesis can be performed using a one-pot approach with VCl_3, lithium, and naphthalene added all at once to THF. After 12 hours, the reaction is finished and resulted in a deep black suspension of V(0) nanoparticles in THF (Fig. 1a). Subsequent to its synthesis, the as-prepared V(0) nanoparticles were centrifuged and purified by repeated redispersion/centrifugation in/from THF. Thereafter, the V(0) nanoparticles are obtained as a powder sample, which can be used to perform reactions with aromatic N-heterocycles (Fig. 1b). Although the reduction of VCl_3 with [LiNaph] or [NaNaph] is similar, it must be noted that LiCl – formed after the reduction of VCl_3 with [LiNaph] – can be removed by repeated redispersion/centrifugation in/
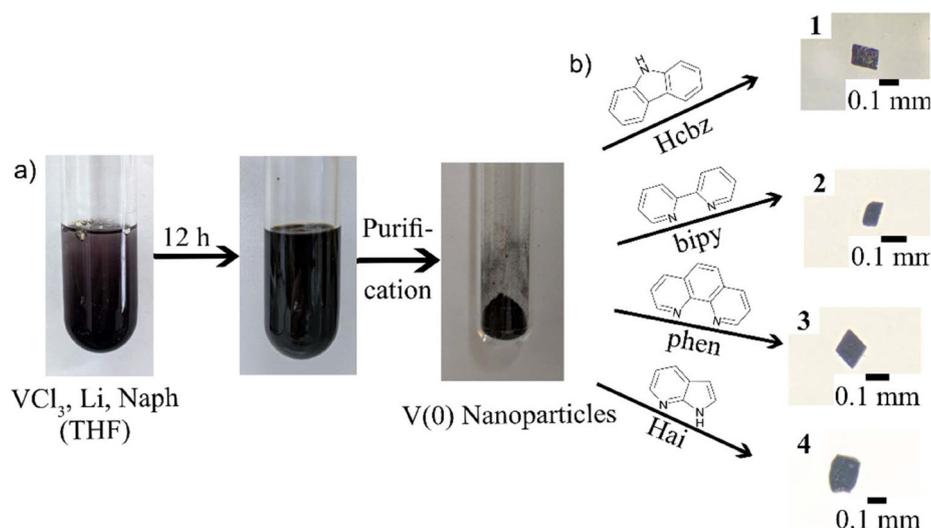
Fig. 1 Scheme illustrating the reactions of V(0) nanoparticles with aromatic N-heterocycles: (a) synthesis of V(0) nanoparticles, and (b) reaction of the as-prepared V(0) nanoparticles with carbazole (Hcbz), 2,2′-bipyridine (bipy), 1,10-phenanthroline (phen) and 7-azaindole (Hai) (photographs on the right show single crystals of the compounds **1–4**).

from THF. In contrast, NaCl – formed after the reduction of VCl_3 with [NaNaph] – is almost insoluble in THF and cannot be removed after the synthesis. As shown in previous studies, LiCl and NaCl are usually not included in the products,[2–6] and thus, our intention was to reduce the time and effort of purification (*i.e.* multiple centrifugation cycles in a glovebox) and confine the redispersion/centrifugation steps in/from THF to just one iteration. Therefore, the V(0) nanoparticles do contain either LiCl or NaCl (SI: Fig. S1).

The size and size distribution of the as-prepared V(0) nanoparticles were examined *via* scanning transmission electron microscopy (STEM). STEM overview images show small-sized nanoparticles with a spherical shape and narrow size distribution (Fig. 2a). A statistical evaluation of approximately 200 particles on STEM images indicated an average diameter of 1.6

± 0.3 nm (Fig. 2b). At the level of experimental significance, the size and size distribution of the nanoparticles are independent of the applied reducing agent [LiNaph] or [NaNaph].[4b,6]

The surface functionalization of the V(0) nanoparticles was investigated using Fourier transform infrared (FT-IR) spectroscopy, elemental analysis (EA), and thermogravimetry (TG). FT-IR spectra predominantely show weak vibrations related to naphthalene and THF (Fig. 3a). Thus, ν(C–H) at 3055 cm^{-1} as well as the fingerprint area with vibrations at 1384, 1343, 1171, 1138, 990, and 618 cm^{-1} indicate the presence of naphthalene. Hereof, the out-of-plane bending vibration at 745 cm^{-1} is the most characteristic and in good agreement with the spectral signal for pure naphthalene shown as a reference (775 cm^{-1}, Fig. 3a).[10] The presence of THF is indicated by ν(C–H) at 2979 and 2878 cm^{-1} and ν(C–O) at 1068 and 897 cm^{-1}, which is
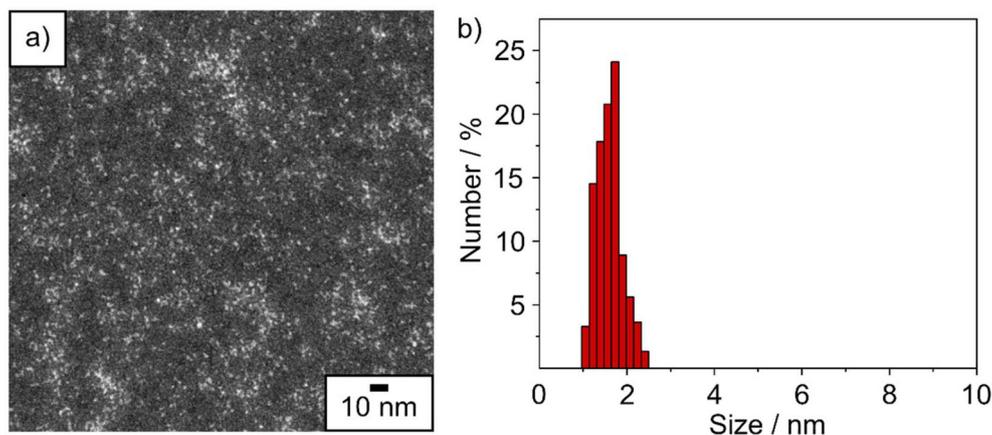

Fig. 2 Size and size distribution of the as-prepared V(0) nanoparticles: (a) STEM image and (b) size distribution based on a statistical evaluation of >200 nanoparticles on STEM images.
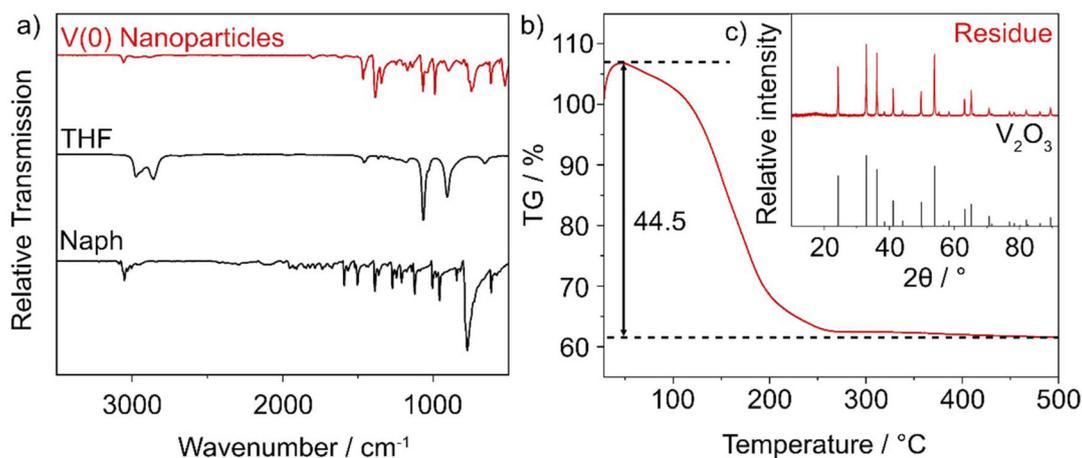
Fig. 3 Surface functionalisation of the V(0) nanoparticles. (a) FT-IR spectrum (references: THF, naphthalene), (b) TG (nitrogen atmosphere), and (c) X-ray powder diffractogram of the thermal remnant (reference: V_2O_3 with ICDD-No. 00-34-0187).

comparable to the values of the pure THF reference spectrum (Fig. 3a). This adsorption of THF/naphthalene on the particle surface is to be expected for nanoparticles synthesized in the liquid phase. Notably, O–H vibrations ($3600–3200$ cm^{-1}) are not observed, which points to the absence of any moisture. EA (C/H/N/S analysis) shows carbon and hydrogen contents of 49.3 and 4.2%, respectively. Here, the C : H ratio of 11.7 indicates preferred surface functionalization of the V(0) nanoparticles with naphthalene (C : H = 15) rather than with THF (C : H = 6). Finally, TG analysis under nitrogen shows an instantaneous increase in mass after starting the measurement, which can be attributed to the oxidation of the V(0) nanoparticles by oxygen. Thereafter, a continuous mass loss of 44.5% is observed up to 250 °C due to the release of surface-adsorbed naphthalene and THF (Fig. 3b). Finally, the thermal residue was identified *via* X-ray powder diffraction (XRD) as V_2O_3 (Fig. 3c).

As an organic content of 45% seems to be high at first sight, we estimated the expected organic content with the assumption of a monomolecular layer of naphthalene adsorbed on the surface of the as-prepared V(0) nanoparticles. First of all, account must be taken that about 90% of all vanadium atoms are located on the particle surface with a mean nanoparticle size of 1.6 ± 0.3 nm.[11] At this diameter, a single V(0) nanoparticle exhibits a surface area of 8.0 nm^2 and a volume of 2.1 nm^3. Based on a density of 6.1 g cm^{-3} or 6.1×10^{-18} mg nm^{-3} for bulk vanadium,[12] a volume of 2.1 nm^3 relates to a mass of 12.8×10^{-18} mg for V. Furthermore, the area of a naphthalene molecule can be deduced as being 0.6×0.3 nm = 0.18 nm^2.[13] A flat adsorption of naphthalene molecules on the surface of a V(0) nanoparticle would then result in 44 naphthalene molecules undergoing monomolecular adsorption. These 44 molecules of naphthalene ($M = 128\,000$ mg mol^{-1}) have a mass of 9.4×10^{-18} mg, which corresponds to the organic content being about 43% of the total nanoparticle mass (12.8×10^{-18} mg V + 9.4×10^{-18} mg

naphthalene) due to the assumed monomolecular adsorption of naphthalene on the nanoparticle surface. Although this rough estimation has several weaknesses (*e.g.*, size distribution of nanoparticles, density of nanomaterial lower than bulk, potential side-on or end-on adsorption of naphthalene, additional THF adsorption on the particle surface, *etc.*), the order of magnitude is in good agreement with the experimental results of about 40–50% according to TG and EA.

### 3.2 Reactions with N-heterocycles

Due to both the stability in different oxidation states (+II to +V) and the nitrophilicity of vanadium,[14] V(0) nanoparticles appear to be the most suitable for redox reactions with N-heterocycles to evaluate the formation of new coordination compounds, the oxidation state of vanadium and the coordinative scenario of the different ligands. As representative examples of sterically demanding N–H-acidic/non-N–H-acidic, chelating/non-chelating aromatic N-heterocycles, we selected carbazole (Hcbz), 2,2′-bipyridine (bipy), 1,10-phenanthroline (phen), and 7-azaindole (Hai) (*cf.* Fig. 1). These N-heterocycles are widely applied as ligands and are well known for their flexible coordination to form a wide range of coordination compounds.[15] Although numerous coordination compounds have been described, the homoleptic coordination of metal cations by these respective N-heterocycles is rare. Usually additional ligands (including solvent molecules) are involved.

As general observations, it should first be noted that V(0) nanoparticles, obtained by reduction of VCl_3 with [LiNaph], did not yield any crystalline compounds or visible reactions. This behavior is most likely attributable to coordination of the N-heterocycles to lithium, another nitrophilic cation with high charge density. The resulting compounds obviously remain in solution. In contrast, V(0) nanoparticles generated by reduction of VCl_3 with [NaNaph] reacted with all applied N-heterocycles to afford compounds **1–4**. Remarkably, despite the presence of NaCl, Na^+ was incorporated only in compound

1. Finally, the growth of suitable single crystals, specifically those of compounds **1** and **4** containing N–H-acidic N-heterocycles, required a certain time, although the reactions leading to formation of **1–4** were fast in principle.

All reactions of V(0) nanoparticles with the respective N-heterocyclic agents were performed in toluene at 80–120 °C. Toluene (tol) appeared to be the most suitable liquid phase as it weakly coordinates with itself and guarantees good solubility of the N-heterocycles. First, carbazole (Hcbz) was used as a representative example of a widely applied, sterically demanding, N–H-acidic ligand. Its reaction resulted in quadratic crystals that – according to X-ray single-crystal structure analysis – crystallize in the monoclinic space group $C2/c$ (SI: Table S1) with a composition denoted by $[NaV(cbz)_4]$ (SI: Fig. S2). The Na^+ cations originate from NaCl as a by-product of the reduction of VCl_3 with $[NaNaph]$. The formation of **1** can be described as follows:

$$4V + 12Hcbz + 3NaCl \rightarrow 3[NaV(cbz)_4] + VCl_3 + 6H_2$$
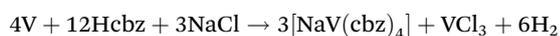
Compound **1** contains V(III) with tetrahedral coordination of four cbz^- ligands (Fig. 4a). The V–N distances range from 196.5(1) to 198.3(2) pm (Table 1). The N–V–N bond angles (104.3(1)–114.7(1)°) confirm the distorted tetrahedral arrangement. Both the V–N distances and the N–V–N angles point to the deprotonation of Hcbz and the presence of negatively

Table 1 Comparison of V–N distances in **1–4** relative to the oxidation state of vanadium

Compound	V–N distance (pm)	Oxidation state of vanadium
$[NaV(cbz)_4]$ (**1**)	196.5(6)–198.3(2)	+III
$[V(bipy)_3]$ (**2**)	204.6(3)–208.7(3)	+III
$[V(phen)_3]$ (**3**)	207.0(3)–209.1(3)	+III
$[V(Hai)_3(ai)_2]\cdot0.5tol$ (**4**)	219.0(2)–225.7(2) (pyridine-N) 216.9(4), 219.0(2) (pyrrole-N)	+II

charged cbz^- in **1**. The V–N distances are also in good agreement with the coordination of vanadium by N-pincer ligands in, for instance, $[V(Cbz)_2(NMe_2)_2Cl_2]$ (V–N: 189.6(2) pm) or $[VCz^{tBu}(Pyr^{iPr})_2(N_3)_2]$ (V–N: 191.0(2) pm).[16] Interestingly, the $[V(cbz)_4]^-$ units in **1** are interconnected to a 2D network via Na^+ cations (Fig. 4a). Na^+ shows η^2 coordination to, in total, four benzene rings of four different cbz^- ligands. The Na–C distances (264.1(2)–287.2(2) pm) are in good agreement with the typical literature values (263–285 pm).[17] In contrast, significantly longer Na–C distances are observed for the remaining, non-coordinated C atoms of the benzene rings (320.4(9)–425.9(5) pm). In contrast to previous studies, the redox approach based on V(0) nanoparticles resulted in a homoleptic coordination of V(III) with the deprotonated, sterically demanding
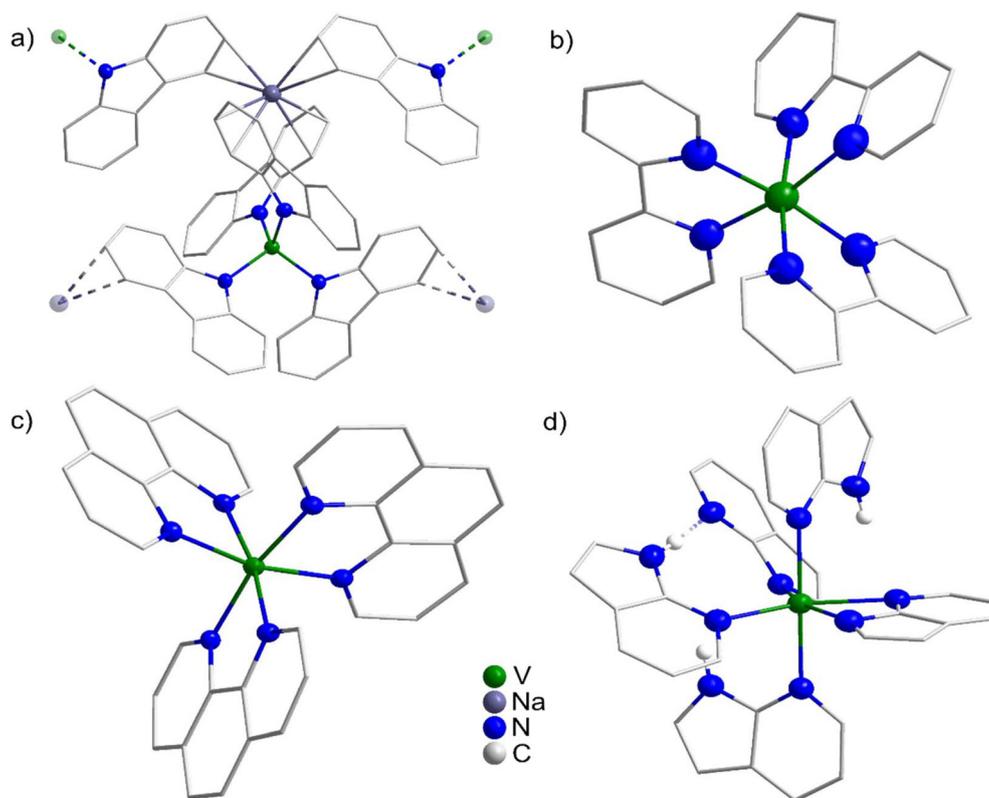

Fig. 4 Molecular structures of vanadium compounds with N-heterocycles: (a) $[NaV(Cbz)_4]$ (**1**), (b) $[V(bipy)_3]$ (**2**), (c) $[V(phen)_3]$ (**3**), and (d) $[V(\eta^1\text{-}Hai)_3(\eta^2\text{-}ai)(\eta^1\text{-}ai)]\cdot0.5$ tol (**4**).

cbz⁻ anions and without the involvement of any other organic molecule, solvent or halide as additional ligands. Carbazole and its derivatives are generally well-known as ligands, showing adaptable η^1 to η^6 coordination.[18] Most often, they have been used as pincer ligands to coordinate single metal atoms. The deprotonation of the N–H group is usually performed by the reaction with silylamides or alkali metals. Complexes of cbz⁻ and vanadium, to the best of our knowledge, have not been described until now.

As a second N-heterocycle, 2,2′-bipyridine (bipy) was reacted with the V(0) nanoparticles. Bipy is well-known as a bidentate chelating ligand,[19] has a comparable size to HCbz, but is not N–H acidic. Here, the reaction of V(0) nanoparticles resulted in black crystals of composition [V(bipy)₃] (**2**) and, again, displaying homoleptic coordination, according to the following reaction:

$$V + 3bipy \rightarrow [V(bipy)_3]$$
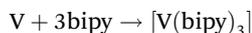
Based on X-ray single-crystal structure analysis, **2** crystallizes in the space group $P2_1/c$ (SI: Table S2 and Fig. S3). In **2**, vanadium shows a distorted octahedral coordination with three μ^2-binding bipy ligands and V–N distances of 204.6(3)–208.7(3) pm (Table 1 and Fig. 4b). In the solid state, the non-charged molecular [V(bipy)₃] units are arranged according to primitive cubic packing.

In fact, reactions and coordination of vanadium and bipy ligands, including the composition [V(bipy)₃], have been long-known and intensely studied with regard to their bonding situation.[20] Initial syntheses were reported by Herzog[20a] and Albrecht,[20b] who obtained [V(bipy)₃] by the reduction of [V(II)(bipy)₃]I₂ with magnesium or zinc. Despite having a similar molecular structure, they reported that the compound crystallizes in the space group $P3c$ or $P6/mmm$, both of which are different from $P2_1/c$ observed for **2** (SI: Table S2). With regard to its bonding situation, [V(bipy)₃] was assumed to represent an analogue of the chemically less stable zerovalent vanadium carbonyl [V(±0)(CO)₆].[20] Besides the non-charged molecule, charged species like [V(bipy)₃]²⁺, [V(bipy)₃]⁺, and [V(bipy)₃]⁻ have also been reported.[21] Electron paramagnetic resonance (EPR) spectroscopy ultimately pointed to an oxidation state of V(III) in the non-charged species [V(bipy)₃].[22] Following precise analysis of the interpyridyl C_{py}–C_{py} distances and the pyridyl-N–C distances by Wieghardt et al.,[23] we also concluded that **2** contains V(III) and bipy⁻ anions. Thus, C_{py}–C_{py} distances of 142.8(6)–144.6(7) pm and N–C distances of 135.1(6)–140.1(6) pm in **2** are in good agreement with the literature data of the monoanionic bipy⁻ radical (C_{py}–C_{py}: 142–144 pm; N–C: 138–140 pm).[23] This finding is also in accordance with the V–N distances of **1** and **2** (Table 1), which are significantly shorter for **1** due to the localization of the negative charge only on the nitrogen atom of cbz⁻, whereas the negative charge is delocalized over the whole bipy⁻ anion in **2**.

In addition to bipy, the even larger, non-N–H-acidic, bidentate 1,10-phenanthroline (phen) was reacted with the V(0) nanoparticles according to the following reaction leading to the formation of [V(phen)₃] (**3**). Compound **3** crystallizes as

black crystals in the monoclinic space group $P2_1/n$ (SI: Table S3 and Fig. S4):

$$V + 3phen \rightarrow [V(phen)_3]$$
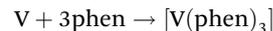
Similar to **2**, vanadium in **3** is distorted octahedrally and coordinated by three phen ligands (Fig. 4c). Phen serves as a bidentate ligand with V–N distances of 207.0(3) to 209.1(3) pm, which are comparable to the V–N distances in **2** (Table 1). Based on the similar synthesis strategy, similar coordination and comparable V–N distances observed for **2**, compound **3** can also be assumed to contain V(III), which is coordinated homoleptically with three monoanionic phen⁻ ligands.

In fact, a [V(phen)₃] product has already been reported in the literature and prepared either by the reduction of [V(phen)₃]Br₂ with [LiPh₂CO] or by the reduction of VCl₃/phen with sodium amalgam.[20d,24] However, a crystal-structure analysis was not performed, and the vanadium was designated as being zerovalent. Moreover, cationic species such as [V(II)(phen)₃]²⁺ were described, containing phen as a non-charged ligand.[21a,c,d] Furthermore, coordination compounds of vanadium and phen include vanadium with other oxidation states (V(II) and V(IV)), other ligands in addition to phen, and phen always present as a non-charged ligand.[25] In particular, V(IV)-containing compounds were evaluated as potential chemotherapeutic agents.[25d–f]

Finally, the V(0) nanoparticles were reacted with 7-azaindole (7-Hai). As an N-heterocycle that is both bidentate and N–H-acidic, 7-Hai combines the features of the aforementioned Hcbz, bipy, and phen ligands. In principle, this offers different options for cation coordination via a single or via both N atoms as well as with or without deprotonation of the N–H function (Fig. 5).[26] According to the literature, various coordination scenarios are described. Thus, 7-Hai often shows deprotonation with the formation of dinuclear metal complexes via μ-N,N-coordination.[27] Mononuclear complexes most often exhibit monodentate coordination via the pyridine-N atom.[28] In contrast, metal coordination via the pyrrole-N has been reported less often.[29] A bidentate μ-N,N or η^2-N,N-coordination of 7-Hai is generally rare but has been reported, for instance, with Cu²⁺ or Yb²⁺, respectively (Fig. 5).[30] With particular aim on Hai complexes of vanadium, other ligands in addition to 7-Hai were required.[31]

The reaction of V(0) nanoparticles with 7-Hai at 100 °C resulted in dark red crystals. According to X-ray single-crystal structure analysis, the compound was identified as [V(η^1-Hai)₃(η^2-ai)(η^1-ai)]·0.5 tol (**4**), which crystallizes in the triclinic space group $P\bar{1}$ according to the following reaction (SI: Table S4 and Fig. S5):

$$V + 5Hai + 0.5tol \rightarrow [V(\eta^1\text{-Hai})_3(\eta^2\text{-ai})(\eta^1\text{-ai})] \cdot 0.5tol + H_2$$

In **4**, vanadium is coordinated in a distorted octahedral geometry by five 7-Hai/7-ai⁻ ligands (N–V–N bond angles: 86.3(1)–178.9(1)°; Fig. 4d). Besides the molecular [V(η^1-Hai)₃(η^2-ai)(η^1-ai)] structure, 0.5 molecules of toluene (tol) are present per formula unit, located between the vanadium complexes (SI:
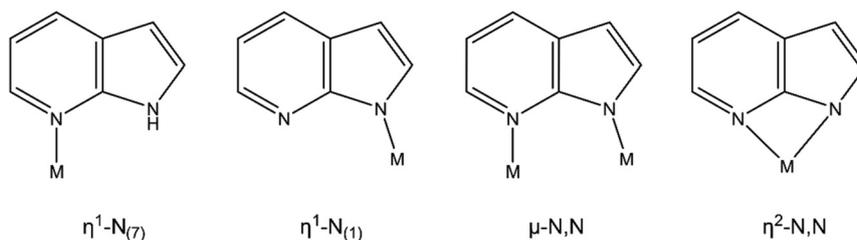
Fig. 5 Possible coordination scenarios of the 7-Hai ligand (modified from ref. 26).

Fig. S5). This tol molecule shows positional disorder, which was modelled by split-atom positions for all atoms with an occupancy for each of 50%. The non-charged molecular [V(η^1-Hai)$_3$(η^2-ai)(η^1-ai)] units are (similar to **1**) arranged in a primitive cubic packing.

Surprisingly, the coordination of the five Hai/ai$^-$ ligands is very different (Fig. 4d). Four Hai/ai$^-$ ligands coordinate with vanadium *via* their pyridine-N atom with V–N distances of 219.0(2)–225.7(2) pm (Table 1; SI: Fig. S6), whereas one Hai/ai$^-$ ligand only coordinates with vanadium *via* the pyrrole-N atom with a V–N distance of 216.9(2) pm (Table 1; SI: Fig. S6).

Furthermore, four Hai/ai$^-$ ligands serve as monodentate ligands, whereas only one is bidentate and coordinates *via* the pyridinic N atom (V–N: 225.7(2) pm) as well as the pyrrolic N atom (V–N: 219.0(2) pm). The shorter V–N distances of the pyrrolic N atoms in comparison to the pyridinic N atoms and the observation that only two pyrrolic N atoms coordinate to vanadium point to the fact that these two pyrrolic N atoms are deprotonated, whereas the three non-coordinating pyrrolic N atoms remain protonated. For the ai$^-$ ligand coordinating *via* a pyrrolic N atom only, hydrogen bonding of the pyridinic N atom to a neighbouring pyrrolic NH function is observed (N–
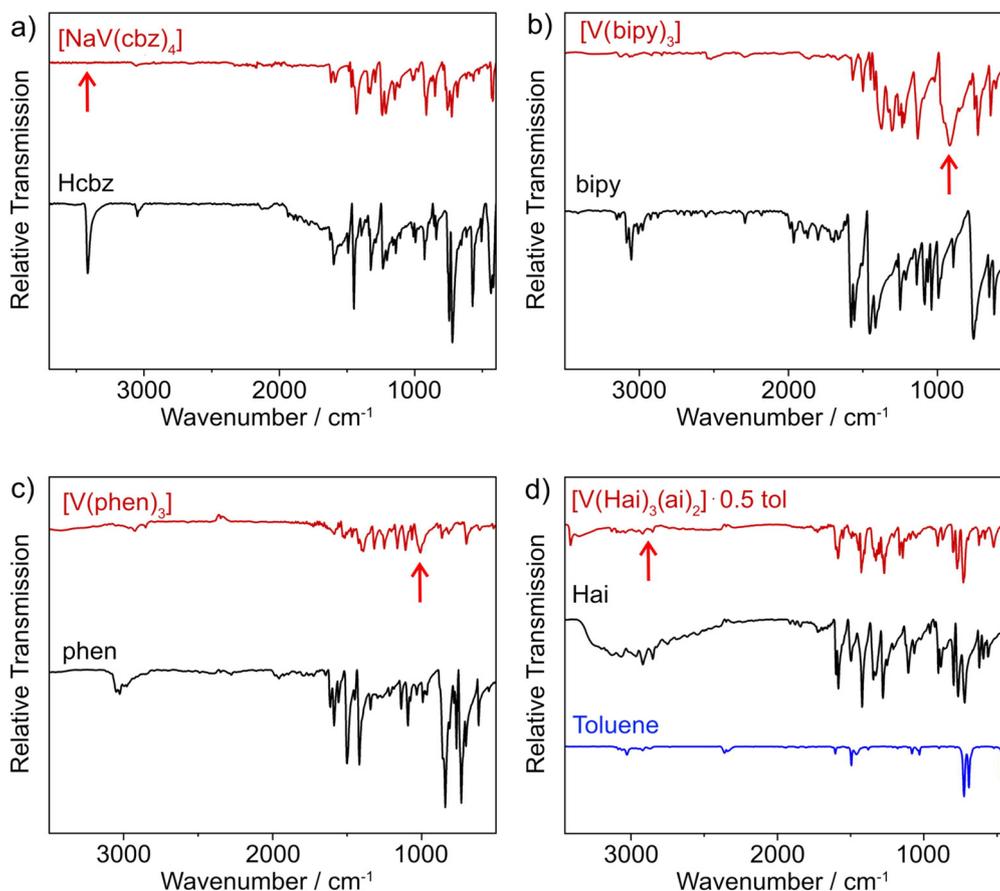

Fig. 6 FT-IR spectra of (a) [NaV(cbz)$_4$] (**1**) (with pure Hcbz as a reference), (b) [V(bipy)$_3$] (**2**) (with pure 2,2′-bipy as a reference), (c) [V(phen)$_3$] (**3**) (with pure 1,10-phen as a reference), and (d) [V(Hai)$_3$(ai)$_2$]·tol (**4**) (with pure 1,7-Hai and toluene as references). Red arrows indicate specific vibrations explained in the discussion.

H···N: 191.0(2) pm; Fig. 4d). Finally, based on three neutral Hai ligands and two monoanionic ai$^-$ ligands, the oxidation state of vanadium is determined as being V(ɪɪ) in **4**. In summary, such flexible and homoleptic coordination of 7-Hai/7-ai$^-$ ligands with three different options – including η^1-Hai, η^2-ai$^-$, or η^1-ai$^-$ – combined in one molecular complex are observed herein for the first time.

3.3 Properties of coordination compounds 1–4

In addition to single-crystal structure analysis, X-ray powder diffraction (XRD) with Rietveld refinement was performed to verify the space group and crystallography data of the title compounds (SI: Fig. S7). To this end, the data obtained from single-crystal structure analysis were used as a starting model for the Rietveld refinement. Based on the refinement, an additional phase was identified, which turned out to be NaCl. NaCl originates from the synthesis of the V(0) nanoparticles and cannot be removed thereafter due to its poor solubility in THF or toluene. Besides the NaCl by-product, the experimental diffractograms are in good agreement with the Rietveld refinement, which confirms the crystal structure and symmetry of the respective title compounds (SI: Fig. S7). Due to the sticki-

ness of the title compounds, filling capillaries for XRD analysis required mixing them with dried quartz powder, which, on the one hand, resulted in higher background interference due to amorphous material and, on the other hand, reduced the scattering intensity. As a result, the data quality was not sufficient to perform Rietveld refinements of compound **1** (SI: Fig. S7a). The powder diffraction data nevertheless show good agreement with diffractograms calculated based on the data from single-crystal structure analysis.

FT-IR spectra of the title compounds **1–4** are compared with spectra of the pure N-heterocycles to verify their presence and coordination (Fig. 6). Accordingly, **1–4** show the characteristic vibrations of the respective ligand. These vibrations are partly shifted to higher wavenumbers, which can be attributed to the coordination of the N-heterocycle to the vanadium cation. In the case of **1**, the absence of any ν(N–H) vibration bands (3415 cm^{-1}) points to the deprotonation of the cbz$^-$ ligand (Fig. 6a: red arrow). Furthermore, the ν(C–H) vibrations at 3053 cm^{-1}, the δ(C–H) vibrations at 1430 cm^{-1} and the ring vibrations at 758 and 727 cm^{-1} can all be assigned to the deprotonated carbazole ligand. For **4**, only two of the five ligands are deprotonated (Fig. 6d). Therefore, the ν(N–H) vibration (3200–3080 cm^{-1}) is still visible but shows a reduced
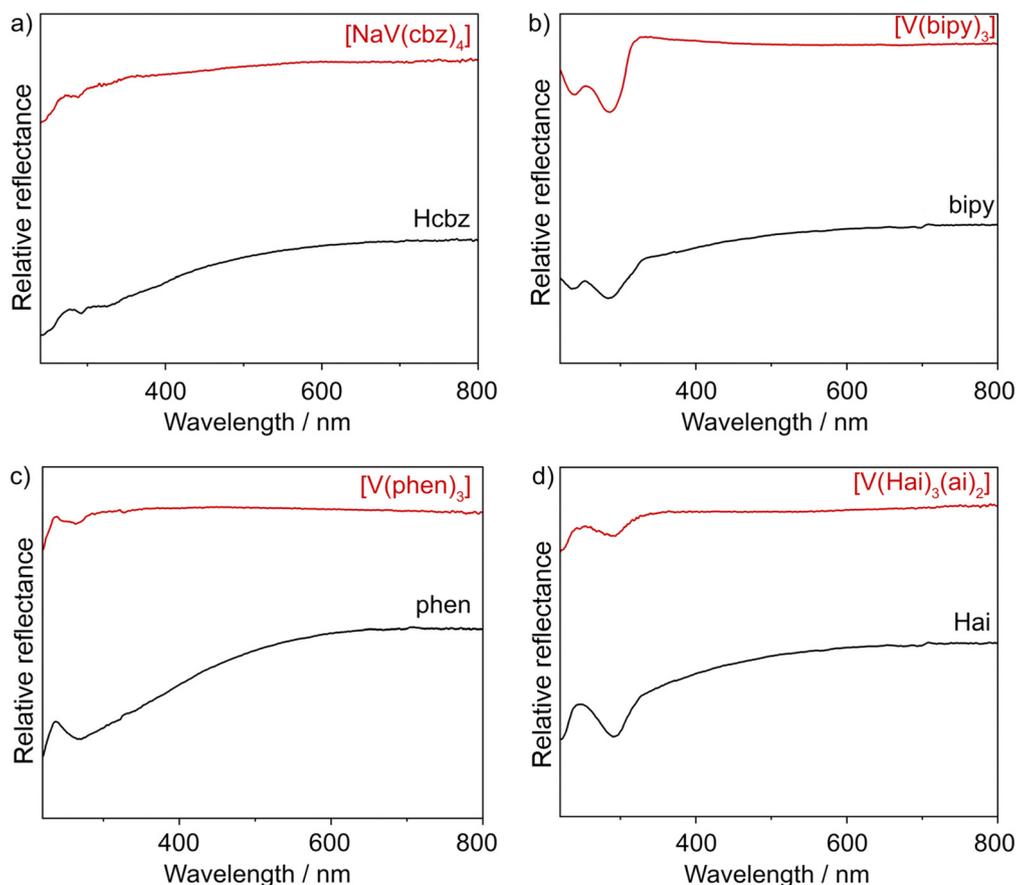

Fig. 7 UV-Vis spectra of (a) [NaV(cbz)$_4$] (**1**) (with pure Hcbz as a reference), (b) [V(bipy)$_3$] (**2**) (with pure 2,2′-bipy as a reference), (c) [V(phen)$_3$] (**3**) (with pure 1,10-phen as a reference), and (d) [V(Hai)$_3$(ai)$_2$]·tol (**4**) (with pure 1,7-Hai as a reference).

intensity in comparison with pure Hai, which is in accordance with partial deprotonation (Fig. 6d: red arrow). The ν(C–C) vibrations below 1600 cm^{-1} and the δ(C–H) vibrations at 800, 773 and 731 cm^{-1} confirm the presence of the Hai/ai$^-$ ligands. Furthermore, the ring vibration at 464 cm^{-1} can be attributed to toluene, which is located between the molecular [V(Hai)$_3$(ai)$_2$] units of **4** (SI: Fig. S5). For **2**, the characteristic vibrations of the bipy$^-$ radical anion are significantly shifted in comparison with the non-charged bipy molecule (Fig. 6b). Such a shift is well-known in the literature and related to the localization of the additional electron in an anti-bonding π^* orbital.[32] Characteristic vibrations of the bipy$^-$ radical anion comprise ν(C=N) and ν(C=C) vibrations at 1490, 1415, 1370, and 1285 cm^{-1} as well as the intense ring-deformation band at approximately 950 cm^{-1}, which is specific to the radical state (Fig. 6b: red arrow). A similar shift of vibrations is also observed for the phen$^-$ radical anion in comparison with the non-charged phen molecule (Fig. 6c). These shifts are again in agreement with the literature. The intense ring-deformation band at approximately 1012 cm^{-1} is specifically a characteristic of the radical state (Fig. 6c: red arrow).[33]

Finally, the optical properties of the title compounds **1–4** were monitored based on UV-Vis spectra (Fig. 7). Although single crystals only show a less specific dark greyish colour (compare Fig. 1), characteristic absorptions are observed for all title compounds. The absorption can be ascribed to the respective N-heterocycles that are displayed as well as references. The characteristic absorption of the ligands at 250–350 nm occurs for both the respective title compound and the pure ligand.

4. Conclusions

Four novel compounds [NaV(cbz)$_4$] (**1**), [V(bipy)$_3$] (**2**), [V(phen)$_3$] (**3**), and [V(Hai)$_3$(ai)$_2$]·0.5tol (**4**) have been prepared and characterized by X-ray diffraction (single crystal and powder) as well as by spectroscopic methods (FT-IR and UV-Vis). **1–4** represent homoleptic coordination compounds with distorted tetrahedral (**1**) or distorted octahedral (**2–4**) coordination of vanadium by nitrogen-donor atoms of the sterically demanding N–H-acidic/non-N–H-acidic, chelating/non-chelating aromatic N-heterocycles carbazole (Hcbz), 2,2′-bipyridine (bipy), 1,10-phenanthroline (phen), and 7-azaindole (Hai). The title compounds were prepared *via* a redox approach using V(0) nanoparticles (mean size: 1.6 ± 0.3 nm) as a reactive starting material and by direct reaction with the N-heterocycles in toluene at 80–120 °C. Whereas **2–4** consist of molecular homoleptic building units with V(III) (**2,3**) and V(II) (**4**) as the central atom, anionic [V(III)(cbz)$_4$]$^-$ units are interconnected *via* Na$^+$ cations, showing η^2-coordination with four benzene rings of cbz, to a 2D network. Of particular interest is compound **4** with three different coordination scenarios of the Hai/ai$^-$ ligand, resulting in a structure of composition [V(η^1-Hai)$_3$(η^2-ai)(η^1-ai)]·0.5tol, which has generally been observed for the first time. In summary, the use of V(0) nanoparticles as

a starting material in a redox approach results in homoleptic coordination with four different N-heterocycles, which, on a broader scope, can also become a suitable, novel synthesis strategy for other metals and ligands.

Conflicts of interest

The authors declare no competing financial interest.

Data availability

Additional data regarding experiments and methods are provided in the supporting information (SI) and can also be obtained upon request from the authors.

All details related to the crystal structures may also be obtained from the joint CCDC/FIZ Karlsruhe deposition service.

Supplementary information: additional information regarding the analytical techniques, details of the single-crystal structure analysis, and further characterization of the title compounds. See DOI: https://doi.org/10.1039/d6dt00230g.

CCDC 2522846–2522849 contain the supplementary crystallographic data for this paper.[34a–d]

References

1 (*a*) F. Gyger, P. Bockstaller, D. Gerthsen and C. Feldmann, *Angew. Chem., Int. Ed.*, 2013, **52**, 12443–12447; (*b*) C. Schöttle, P. Bockstaller, D. Gerthsen and C. Feldmann, *Chem. Commun.*, 2014, **50**, 4547–4550; (*c*) A. Egeberg, T. Block, O. Janka, O. Wenzel, D. Gerthsen, R. Pöttgen and C. Feldmann, *Small*, 2019, **15**, 1902321.

2 (*a*) D. Bartenbach, O. Wenzel, R. Popescu, L.-P. Faden, A. Reiß, M. Kaiser, A. Zimina, J.-D. Grunwaldt, D. Gerthsen and C. Feldmann, *Angew. Chem., Int. Ed.*, 2021, **60**, 17373–17377; (*b*) A. Reiß, C. Donsbach and C. Feldmann, *Dalton Trans.*, 2021, **50**, 16343–16352; (*c*) C. Schöttle, P. Bockstaller, R. Popescu, D. Gerthsen and C. Feldmann, *Angew. Chem., Int. Ed.*, 2015, **54**, 9866–9870.

3 (a) A. Reiß, J. Göttlicher, T. Vitova and C. Feldmann, *Inorg. Chem.*, 2025, **64**, 9469–9476; (b) L.-P. Faden, C. Donsbach, R. Popescu, L. Bayarjargal, Y. M. Eggeler, B. Winkler and C. Feldmann, *J. Mater. Chem. C*, 2025, **13**, 23269–23279; (c) L.-P. Faden, A. Reiß, R. Popescu, C. Donsbach, J. Göttlicher, T. Vitova, D. Gerthsen and C. Feldmann, *Inorg. Chem.*, 2024, **63**, 1020–1034; (d) C. Ritschel, C. Donsbach and C. Feldmann, *Chem. – Eur. J.*, 2024, **30**, e202400418.

4 (a) C. Ritschel, A. Appenzeller, R. Popescu, C. Donsbach, J. O. Wenzel, F. Breher, Y. M. Eggeler, W. Klopper and C. Feldmann, *Angew. Chem., Int. Ed.*, 2025, e202515995; (b) A. Reiß, A. Appenzeller, J. Baur, J. Wenzel, R. Popescu, K. Beuthert, S. Dehnen, Y. M. Eggeler, F. Breher, W. Klopper and C. Feldmann, *Small*, 2025, **21**, 2503498.

5 (a) S. Riegsinger, R. Popescu, D. Gerthsen and C. Feldmann, *Chem. Mater.*, 2024, **36**, 10496–10503; (b) Y.-C. Chen, Y.-K. Hsu, R. Popescu, D. Gerthsen, Y.-G. Lin and C. Feldmann, *Nat. Commun.*, 2018, **9**, 232.

6 A. Reiß, M. K. Reimann, C. Jin, M. Wachter-Lehn, R. K. Kremer, R. Pöttgen, K. Fink, W. Klopper and C. Feldmann, *Dalton Trans.*, 2023, **52**, 17389–17397.

7 (a) C.-C. Yang, W.-L. Huang, Y.-H. Lin, C.-Y. Wenig, Z.-Y. Mo and Y.-Y. Chen, *IEEE Trans. Magn.*, 2011, **47**, 3535–3537; (b) A. B. Phillips, G. Myeni and B. S. Shivaram, *AIP Conf. Proc.*, 2006, **837**, 250–254.

8 R. Zacharia, K. Y. Kim, A. K. M. F. Kibria and K. S. Nahm, *Chem. Phys. Lett.*, 2005, **412**, 369–375.

9 (a) C. Janiak, *Z. Naturforsch., B: J. Chem. Sci.*, 2013, **68**, 1059–1089; (b) E. Redel, R. Thomann and C. Janiak, *Chem. Commun.*, 2008, 1789–1791.

10 C. L. Dodson and J. F. Graham, *J. Phys. Chem.*, 1973, **77**, 2903–2906.

11 D. Vollath, *Nanomaterials – An Introduction to Synthesis, Properties, and Applications*, Wiley-VCH, Weinheim, 2nd edn, 2013, pp. 23.

12 N. N. Greenwood and A. Earnshaw, *Chemistry of the Elements*, Elsevier, Amsterdam, 2nd edn, 1997, pp. 967.

13 F. R. Ahmed and D. W. J. Cruickshank, *Acta Crystallogr.*, 1952, **5**, 852–853.

14 N. N. Greenwood and A. Earnshaw, *Chemistry of the Elements*, Elsevier, Amsterdam, 2nd edn, 1997, pp. 406.

15 (a) S. J. Malthus, S. A. Cameron and S. Brooker, *Coord. Chem. Rev.*, 2016, **316**, 125–161; (b) C. Verma, I. Y. Chandrabhan, L. K. M. O. Goni, S. S. E. Abdelkreem, S. A. Mubarak, H. A. M. Al-Mohsin, A. Alfantazi and M. A. Jafar Mazumder, *Coord. Chem. Rev.*, 2025, **529**, 216433; (c) C. Phen Queffelec, P. B. Pati and Y. Pellegrin, *Chem. Rev.*, 2024, **124**, 6700–6902; (d) A. Dominguez-Martin, M. del Pilar Brandi-Blanco, A. Matilla-Hernandez, H. El Bakkali, V. M. Nurchi, J. M. Gonzalez-Perez, A. Castineiras and J. Niclos-Gutierrez, *Coord. Chem. Rev.*, 2013, **257**, 2814–2838.

16 A. Lugosan, T. Cundari, K. Fleming, D. A. Dickie, M. Zeller, J. Ghannam and W.-T. Lee, *Dalton Trans.*, 2020, **49**, 1200–1206.

17 I. L. Fedushkin, A. N. Lukoyanov, M. Hummert and H. Schumann, *Russ. Chem. Bull. Int. Ed.*, 2007, **56**, 1765–1770.

18 (a) G. Kleinhans, A. J. Karhu, H. Boddaert, S. Tanweer, D. Wunderlin and D. I. Bezuidenhout, *Chem. Rev.*, 2023, **123**(13), 8781–8858; (b) L. S. Merz, J. Ballmann and L. H. Gade, *Eur. J. Inorg. Chem.*, 2020, 2023–2042.

19 C. Verma, I. Y. Yaagoob, L. K. M. O. Goni, S. S. E. Abdelkreem, S. A. Mubarak, H. A. M. Al-Mohsin, A. Alfantazi and M. A. Jafar Mazumder, *Coord. Chem. Rev.*, 2025, **529**, 216433.

20 (a) S. Herzog, *Z. Anorg. Allg. Chem.*, 1958, **294**, 155–180; (b) G. Albrecht, *Z. Chem.*, 1963, **5**, 182–187; (c) R. Pappalardo, *Inorg. Chim. Acta*, 1968, **2**, 209–215; (d) J. Quirk and G. Wilkinson, *Polyhedron*, 1982, **2**, 209–211.

21 (a) R. G. Pearson and O. A. Gansow, *Inorg. Chem.*, 1968, **7**, 1373–1377; (b) T. Saji and S. Aoyagui, *J. Electroanal. Chem.*, 1975, **63**, 405–419; (c) R. D. Dill, R. I. Portillo, S. G. Shepard, M. P. Shores, A. K. Rappé and N. H. Damrauer, *Inorg. Chem.*, 2020, **59**, 14706–14715; (d) J. P. Joyce, R. I. Portillo, C. M. Nite, J. M. Nite, M. P. Nguyen, A. K. Rappe and M. P. Shores, *Inorg. Chem.*, 2021, **60**, 12823–12834.

22 A. L. Rieger, J. L. Scott and P. H. Rieger, *Inorg. Chem.*, 1994, **33**, 621–622.

23 M. Wang, T. Weyhermüller, J. England and K. Wieghardt, *Inorg. Chem.*, 2013, **52**, 12763–12776.

24 S. Herzog and U. Grimm, *Z. Chem.*, 1964, **4**, 32–33.

25 (a) S. J. Heater, M. W. Carrano, D. Rains, R. B. Walter, D. Ji, Q. Yan, R. S. Czernuszewicz and C. J. Carrano, *Inorg. Chem.*, 2000, **39**, 3881–3889; (b) N. Islam, A. A. Kumbhar, A. S. Kumbhar, M. Zeller, R. J. Butcher, M. B. Dusane and B. N. Joshi, *Inorg. Chem.*, 2010, **49**, 8237–8246; (c) J. Szklarzewicz, A. Jurowska, M. Hodorowicz, G. Kazek, M. Gluch-Lutwin, J. Sapa and M. Papiez, *J. Mol. Struct.*, 2021, **1224**, 129205; (d) L. Hernandez, M. L. Araujo, W. Madden, E. Del Carpio, V. Lubes and G. Lubes, *J. Inorg. Biochem.*, 2022, **229**, 111712; (e) M. F. A. Santos, G. Sciortino, I. Correia, A. C. P. Fernandes, T. Santos-Silva, F. Pisanu, E. Garribba and J. Costa Pessoa, *Chem. – Eur. J.*, 2022, **28**, e202200105; (f) S. J. Kavitha, K. Panchanatheswaran, M. R. J. Elsegood, S. H. Dale, Y. G. Yuen and J. H. McNeill, *J. Inorg. Biochem.*, 2025, **270**, 112929.

26 S.-F. Liu, Q. Wu, H. L. Schmider, H. Aziz, N.-X. Hu, Z. Popovic and S. Wang, *J. Am. Chem. Soc.*, 2000, **122**, 3671–3678.

27 (a) M. Tayebani, K. Feghali, S. Gambarotta and G. P. A. Yap, *Inorg. Chem.*, 2001, **40**, 1399–1401; (b) K. Mondal, N. Mukhopadhyay, A. Sengupta, T. Roy and P. Das, *Chem. – Eur. J.*, 2023, **29**, e202203718; (c) F. A. Cotton, D. G. Lay and M. Millar, *Inorg. Chem.*, 1978, **17**, 186–188; (d) J. M. Casas, B. E. Diosdado, J. Fornies, A. Martin, A. J. Rueda and A. G. Orpen, *Inorg. Chem.*, 2008, **47**, 8767–8775.

28 (a) G. A. van Albada, S. Nur, M. G. van der Horst, I. Mutikainen, U. Turpeinen and J. Reedijk, *J. Mol. Struct.*,

2008, **874**, 41–45; (*b*) J. Poitras and A. L. Beauchamp, *Can. J. Chem.*, 1994, **72**, 1675–1683.

29 (*a*) C.-K. Chan, C.-X. Guo, K.-K. Cheung, D. Li and C.-M. Che, *J. Chem. Soc., Dalton Trans.*, 1994, 3677–3682; (*b*) J. Ashenhurst, L. Brancaleon, A. Hassan, W. Liu, H. Schmider, S. Wang and Q. Wu, *Organometallics*, 1998, **17**, 3186–3195; (*c*) J. A. Przyojski, M. L. Kiewit, K. L. Fillman, H. D. Arman and Z. J. Tonzetich, *Inorg. Chem.*, 2015, **54**, 9637–9645.

30 (*a*) K. Mondal, N. Mukhopadhyay, A. Sengupta, T. Roy and P. Das, *Chem. – Eur. J.*, 2023, **29**, e202203718; (*b*) G. B. Deacon, E. E. Delbridge, B. W. Skelton and A. H. White, *Eur. J. Inorg. Chem.*, 1999, 751–762.

31 (*a*) J. J. H. Edema, S. Gambarotta, A. Meetsma, A. L. Spek and N. Veldman, *Inorg. Chem.*, 1991, **30**, 2062–2066.

32 C. Lapouge, O. Poizat and G. Buntinx, *J. Mol. Struct.*, 2008, **872**, 123–128.

33 S. L. Howell and K. C. Gordon, *J. Phys. Chem. A*, 2004, **108**, 2536–2544.

34 (*a*) CCDC 2522846: Experimental Crystal Structure Determination, 2026, DOI: 10.5517/ccdc.csd.cc2qp74t; (*b*) CCDC 2522847: Experimental Crystal Structure Determination, 2026, DOI: 10.5517/ccdc.csd.cc2qp75v; (*c*) CCDC 2522848: Experimental Crystal Structure Determination, 2026, DOI: 10.5517/ccdc.csd.cc2qp76w; (*d*) CCDC 2522849: Experimental Crystal Structure Determination, 2026, DOI: 10.5517/ccdc.csd.cc2qp77x.